

CoTracker: It is Better to Track Together

Nikita Karaev^{1,2} Ignacio Rocco¹ Benjamin Graham¹ Natalia Neverova¹
Andrea Vedaldi¹ Christian Rupprecht²

¹ Meta AI ² Visual Geometry Group, University of Oxford

nikita@robots.ox.ac.uk

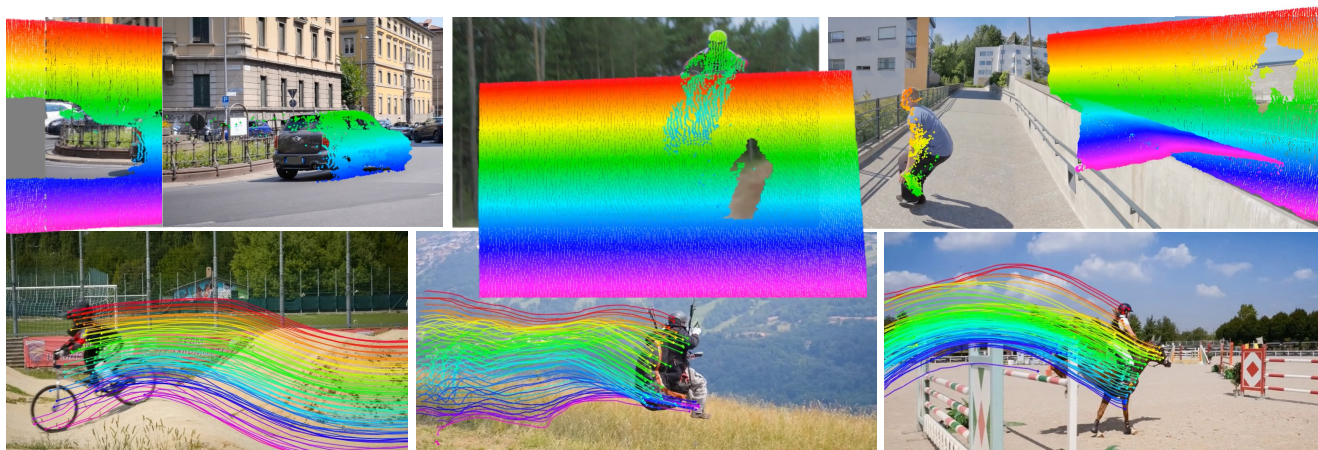


Figure 1. **CoTracker** is a new dense point tracker. It can track 70k points jointly on a single GPU and exploit the correlation between different tracks to improve its performance. It has exceptional long-term tracking performance even in the presence of occlusions or when points leave the camera view (examples from DAVIS [32], the bottom row shows object tracks only).

Abstract

We introduce *CoTracker*, a transformer-based model that tracks dense points in a frame jointly across a video sequence. This differs from most existing state-of-the-art approaches that track points independently, ignoring their correlation. We show that joint tracking results in a significantly higher tracking accuracy and robustness.

We also provide several technical innovations, including the concept of virtual tracks, which allows *CoTracker* to track 70k points jointly and simultaneously. Furthermore, *CoTracker* operates causally on short windows (hence, it is suitable for online tasks), but is trained by unrolling the windows across longer video sequences, which enables and significantly improves long-term tracking.

We demonstrate qualitatively impressive tracking results, where points can be tracked for a long time even when they are occluded or leave the field of view. Quantitatively, *CoTracker* outperforms all recent trackers on standard benchmarks, often by a substantial margin. Code and model weights are available at: <https://co-tracker.github.io/>

1. Introduction

Establishing point correspondences is a fundamental problem in computer vision, necessary for many downstream tasks. Here, we are interested in estimating point correspondences in videos containing dynamic objects and a moving camera. Specifically, given one or more 2D points which are the projection of certain physical points of the underlying 3D scene, the goal is to find the location of the same physical points in all other frames of the video.

There are two variants of this problem. In *optical flow*, the objective is to estimate the velocity of all points within a video frame. This estimation is performed jointly for all points, but the motion is only predicted at an infinitesimal distance. In *tracking*, the goal is to estimate the motion of points over an extended period of time. For efficiency, tracking methods typically focus on a sparse set of points and treat them as statistically independent. Even recent techniques such as TAPIR [11] and PIPs++ [52], which employ modern architectures and can track points even in the presence of occlusions, model tracks independently. However, this approximation is crude as points are often strongly correlated (*e.g.*, when they belong to the same object).

In this paper, we hypothesise that accounting for the correlation between tracked points can significantly improve performance. Thus, we introduce CoTracker, a new neural tracker that, compared to prior deep networks for optical flow and point tracking, supports joint estimation of a very large number of tracks simultaneously. CoTracker outperforms prior trackers on all common tracking benchmarks by substantial margins, is based on a simple and extensible architecture, and is as *flexible* as prior solutions for single-point tracking, meaning that it can track arbitrary points, selected at any spatial location and time in the video, and support arbitrary configurations of such points.

We show that tracking more points jointly significantly improves tracking metrics. In fact, we also show that injecting additional *support points* (*i.e.*, points that are not requested by the user but help the tracker) can further improve performance, and we study several support configurations.

CoTracker achieves its high performance also due to several other innovations in its design and learning formulation. The network is a transformer operating in a sliding window fashion on a two-dimensional representation of tokens, where dimensions are time and the set of tracked points. Via suitable self-attention operators, the transformer can consider each track as a whole for the duration of a window and can exchange information between tracks, thus exploiting their correlation. When tracking a very large number of points, furthermore, CoTracker introduces in its transformer design a small number of representative *virtual track tokens*, switching from expensive self-attention between virtual tracks to cross-attention between the latter and the real ones. This way, CoTracker can jointly track a *near-dense set of tracks* on a single GPU.

Another important contribution is unrolled training. CoTracker is an online algorithm that processes videos in a serial fashion via a sliding window. Within a window, the tracks are initialized with queried points, and the network is tasked with progressively refining these initial estimations through iterative applications of the transformer. Each subsequent overlapping window starts with refined predictions of the previous window and updates tracks for the new frames. We mask out points that have not yet been initialized in the current sliding window, which allows initializing tracks from any point in the video, including in the middle of a window, and to join windows together. We show that, by training the network by unrolling several sliding windows, CoTracker achieves *excellent long-term tracking performance* as well.

We train CoTracker on the synthetic TAP-Vid-Kubric [10] and evaluate it on three different benchmarks, TAP-Vid-DAVIS, PointOdyssey [52] and DynamicReplica [23]. Our architecture works well for tracking single points and excels for groups of points, obtaining state-of-the-art tracking performance in several benchmarks.

2. Related work

Optical flow. Optical flow estimates dense instantaneous motion. Originally approached by studying the colour constancy equation [3, 4, 17, 27], optical flow is nowadays tackled by using deep learning, starting with FlowNet [12, 19]. More recently, DCFlow [48] has introduced the computation of a 4D cost volume, used in most follow-up works [41, 43, 45]. Notable is RAFT [43], which introduced incremental flow updates and inspired a wave of subsequent works [22, 22, 47, 49]. We also adopt 4D cost volumes and iterated updates, but apply them to tracking.

Transformers [44] have also been applied to the optical flow problem [18, 36, 50]. Flowformer [18] drew inspiration from RAFT and proposed a transformer-based approach that tokenizes the 4D cost volume. GMFlow [50] replaced the update network with a softmax with self-attention for refinement. Perceiver IO [20] proposed a unified transformer for several tasks including optical flow.

Optical flow can in principle be applied to tracking by integrating predictions over time, but this open-loop approach accumulates errors in the form of drift, which motivates developing dedicated architectures like ours.

Multi-frame optical flow. There have been several approaches [21, 28, 33, 35] to extend optical flow to multiple frames. Traditionally, Kalman filtering [9, 13] was a staple mechanism to ensure temporal consistency. Modern multi-frame methods produce dense flow. RAFT [43] can be applied in a warm-start manner [39, 42] for multi-frame optical flow estimation. However, these methods are not designed for long-term tracking and do not consider points occluded for a long time. VideoFlow [35] extends optical flow to three and five consecutive frames by integrating forward and backward motion features during flow refinement. MFT [31] conducts optical flow estimation between distant frames and chooses the most reliable chain of optical flows. Our tracker scales to produce semi-dense tracks.

Joint Tracking. Before the emergence of deep learning, some authors proposed handcrafted joint trackers [2, 34], but there is less work on doing so with modern deep network architectures like ours. Our work is weakly related to multiple *object* tracking [8] where tracking through occlusions [51], with changes in appearance [29], and with temporal priors [37] have been extensively studied. However, our focus is the tracking of points, not objects.

Tracking any point. TAP-Vid [10] introduced the problem of tracking any physical point in a video and proposed a benchmark and a simple baseline method for it, but is unable to track occluded points. PIPs [15] revisits the classic Particle Video [34] problem by introducing a model for point tracking through occlusions. The method tracks selected points with a fixed sliding window and restarts from

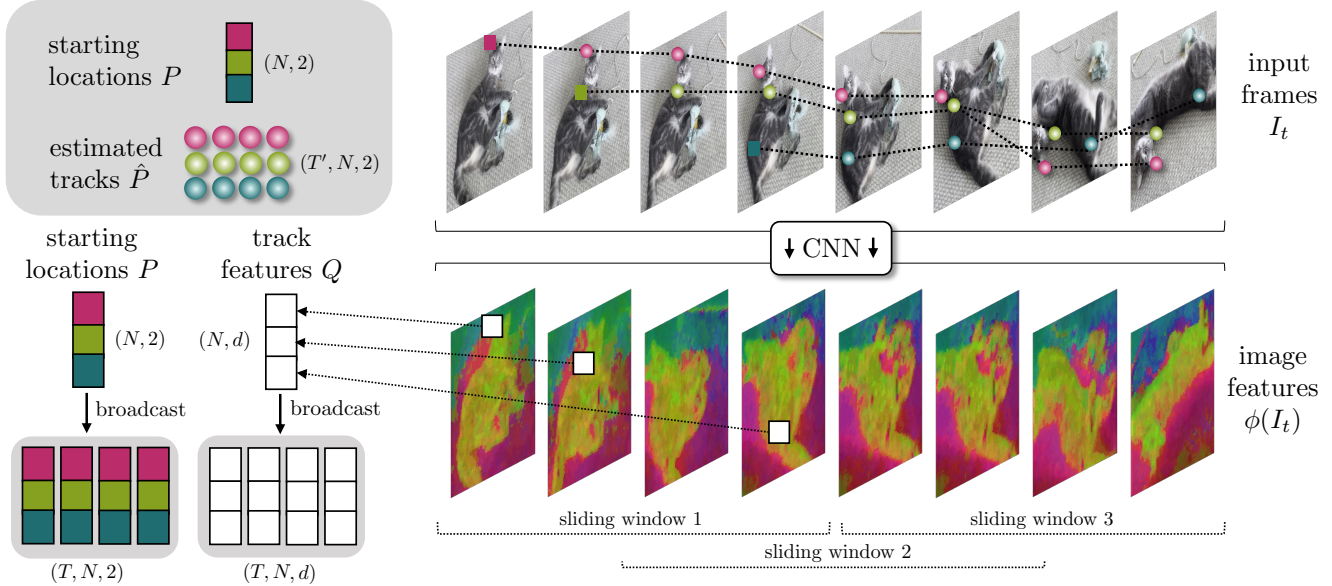


Figure 2. **CoTracker architecture.** We compute convolutional features $\phi(I_t)$ for every frame and process them with sliding windows. In order to initialize track features Q , we bilinearly sample from $\phi(I_t)$ with starting point locations P . Locations P also serve to initialize estimated tracks \hat{P} . See Fig. 3 for a detailed visualization of one sliding window.

the last frame where the point is visible. However, the model loses the target if it stays occluded beyond the size of the window. While the original Particle Video does track points jointly, PIPs and TAP-Vid track points in parallel, but independently. TAPIR [11] proposes a feed-forward point tracker with a matching stage inspired by TAP-Vid [10] and a refinement stage inspired by PIPs [15], which further improves tracking. PointOdyssey [52] addresses long-term tracking with PIPs++, a simplified version of PIPs, and introduces a benchmark for long-term tracking. However, both of these methods still track points independently. OmniMotion [46] optimizes a volumetric representation for each video, refining estimated correspondences in a canonical space. However, this approach requires test-time optimization, which, due to its cost, is not suitable for many practical applications, especially online ones.

Trackers and optical flow estimators are often trained using synthetic datasets [5, 12, 24, 30, 40, 52], as annotating real data can be challenging. Synthetic datasets provide accurate annotations, and training on them has demonstrated the ability to generalize to real-world data [30, 40].

3. CoTracker

Our goal is to track 2D points throughout the duration of a video $V = (I_t)_{t=1}^T$, which is a sequence of T RGB frames $I_t \in \mathbb{R}^{3 \times H \times W}$. The goal of the *tracker* is to predict N point tracks $P_t^i = (x_t^i, y_t^i) \in \mathbb{R}^2$, $t = t^i, \dots, T$, $i = 1, \dots, N$, where $t^i \in \{1, \dots, T\}$ is the time when the track starts. The tracker also predicts the *visibility flag* $v_t^i \in \{0, 1\}$ which

tells if a point is visible or occluded in a given frame. To make the task definition unambiguous [10], we assume each point is visible at the start of their track (*i.e.*, $v_{t^i}^i = 1$). The tracker is thus given as input the video V and the starting locations and times $(P_{t^i}^i, t^i)_{i=1}^N$ of N tracks, and outputs an estimate $(\hat{P}_t^i = (\hat{x}_t^i, \hat{y}_t^i), \hat{v}_t^i)$ of the track locations and visibility for all valid ($t \geq t^i$) times.

3.1. Transformer formulation

We implement the tracker as a transformer neural network (Figs. 2 and 3) $\Psi : G \mapsto O$. The goal of this transformer is to improve an initial estimate of the tracks. Tracks are encoded as a grid of input tokens G_t^i , one for each track $i = 1, \dots, N$, and time $t = 1, \dots, T$. The updated tracks are expressed by a corresponding grid of output tokens O_t^i .

Image features. We extract dense d -dimensional appearance features $\phi(I_t) \in \mathbb{R}^{d \times \frac{H}{k} \times \frac{W}{k}}$ from each video frame I_t using a convolutional neural network (trained end-to-end). We reduce the resolution by $k = 4$ for efficiency. We also consider several scaled versions $\phi_s(I_t) \in \mathbb{R}^{d \times \frac{H}{k2^s-1} \times \frac{W}{k2^s-1}}$, of the features with strides $s = 1, \dots, S$ and use $S = 4$ scales. These downscaled features are obtained by applying average pooling to the base features.

Track features. The appearance of the tracks is captured by feature vectors $Q_t^i \in \mathbb{R}^d$ (these are time-dependent to accommodate changes in the track appearance). They are initialized by sampling image features at the starting locations, and then they are updated by the neural network, as

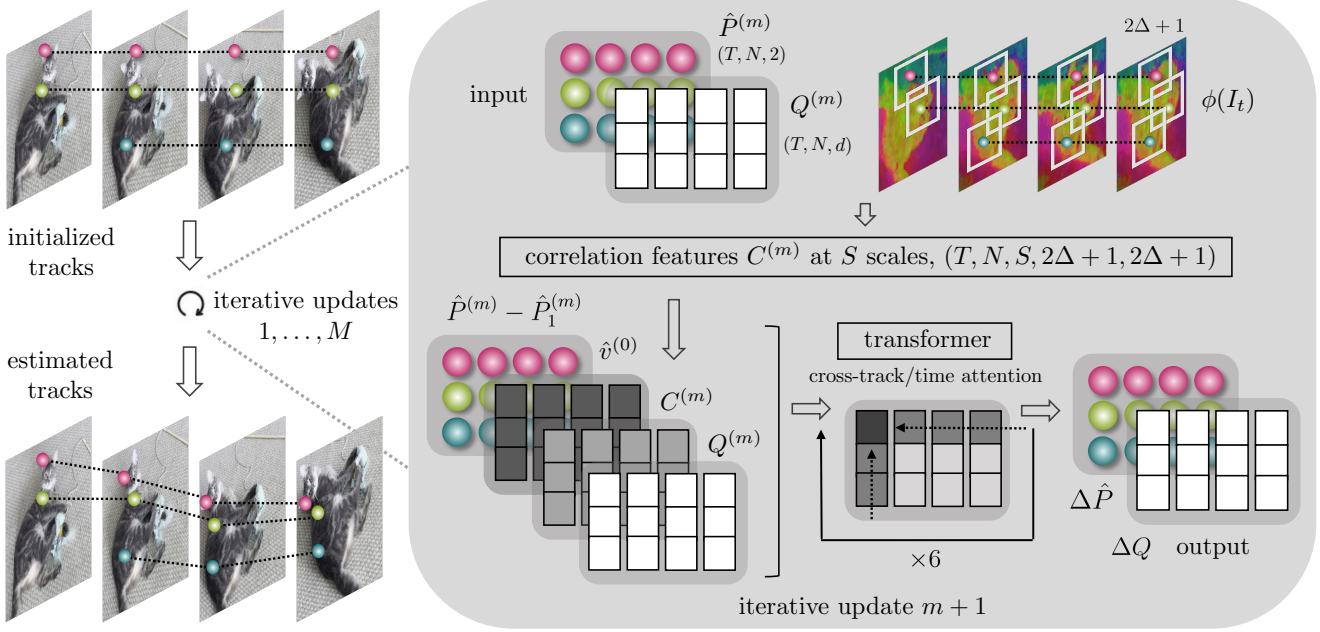


Figure 3. **CoTracker architecture.** Visualization of one sliding window with M iterative updates. During one iteration, we update point tracks $\hat{P}^{(m)}$ and track features $Q^{(m)}$. $Q^{(0)}$ is initialized with the initially sampled features Q for all sliding windows, $\hat{P}^{(0)}$ with the starting locations for the first window. For other windows, $\hat{P}^{(0)}$ starts with predictions for frames processed in the preceding sliding window, and with the last predicted positions for the unseen frames. We compute visibility \hat{v} after the last update M .

explained below.

Correlation features. In order to facilitate matching tracks to images, we adopt the correlation features $C_t^i \in \mathbb{R}^S$ of RAFT [43]. Each C_t^i is obtained by comparing the track features Q_t^i to the image features $\phi_s(I_t)$ around the current estimate \hat{P}_t^i of the tracks’s location. Specifically, the vector C_t^i is obtained by stacking the inner products $[C_t^i]_{s\delta} = \langle Q_t^i, \phi_s(I_t)[\hat{P}_t^i/k_s + \delta] \rangle$, where $s = 1, \dots, S$ are the feature scales and $\delta \in \mathbb{Z}^2, \|\delta\|_\infty \leq \Delta$ are offsets. The image features $\phi_s(I_t)$ are sampled at non-integer locations by using bilinear interpolation and border padding. The dimension of C_t^i is $(2\Delta + 1)^2 S = 196$ for our choice $S = 4; \Delta = 3$.

Tokens. The input tokens $G(\hat{P}, \hat{v}, Q)$ code for position, visibility, appearance, and correlation of the tracks and is given by the following concatenation of features:

$$G_t^i = (\hat{P}_t^i - \hat{P}_1^i, \hat{v}_t^i, Q_t^i, C_t^i, \eta(\hat{P}_t^i - \hat{P}_1^i)) + \eta'(\hat{P}_1^i) + \eta'(t). \quad (1)$$

All the components except the last one have been introduced above. The last component is derived from the estimated position: it is the sinusoidal positional encoding η of the track location with respect to the initial location at time $t = 1$. We also add encodings η' of the start location P_1^i and for the time t , with appropriate dimensions. In fact, we found it beneficial to separately encode the position of points at the first frame and their relative displacement to this frame.

The output tokens $O(\Delta \hat{P}, \Delta Q)$ contain updates for location and appearance, *i.e.* $O_t^i = (\Delta \hat{P}_t^i, \Delta Q_t^i)$.

Iterated transformer applications. We apply the transformer M times in order to progressively improve the track estimates. Let $m = 0, 1, \dots, M$ index the estimate, with $m = 0$ denoting initialization. Each update computes

$$O(\Delta \hat{P}, \Delta Q) = \Psi(G(\hat{P}^{(m)}, \hat{v}^{(0)}, Q^{(m)})).$$

and sets $\hat{P}^{(m+1)} = \hat{P}^{(m)} + \Delta \hat{P}$ and $Q^{(m+1)} = Q^{(m)} + \Delta Q$. The visibility mask \hat{v} is not updated by the transformer, but once after the last of the M applications of the transformer as $\hat{v}^{(M)} = \sigma(WQ^{(M)})$, where σ is the sigmoid activation function and W is a learned matrix of weights. We found iterative updates for the visibility did not further improve the performance, likely due to the fact that visibility highly depends on predicting an accurate location first.

For $m = 0$, the estimates $\hat{P}^{(0)}$, $\hat{v}^{(0)}$ and $Q^{(0)}$ are initialized by broadcasting the initial values $P_{t^i}^i$ (the location of query point), 1 (meaning visible) and $\phi(I_{t^i})[P_{t^i}^i/k]$ (the appearance of the query point) to all times $t = 1, \dots, T$.

3.2. Transformer architecture and virtual tracks

The transformer Ψ interleaves attention operators that operate across the *time* and *track dimensions*, respectively. Factorising the attention [1] across time and tracks makes the model computationally tractable: the complexity is reduced from $O(N^2 T^2)$ to $O(N^2 + T^2)$. However, for very

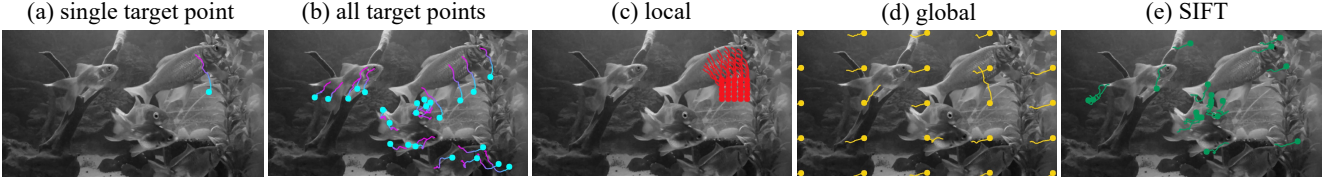


Figure 4. **Tracked and support points.** We visualize different configurations of points along with their tracks. Points represent the start of each track, which clearly illustrates grids of points in (c) and (d). (a) A single target point in a sequence from TAP-Vid-DAVIS. (b) All target points — observe that they tend to cluster on objects of interest, potentially giving our tracker an ‘unfair’ advantage compared to single-track methods. (c) A local grid of support points. (d) A global grid of support points. (e) SIFT support points. We evaluate CoTracker by combining different configurations of support points, as described in Sec. 3.5

large values of N , this cost is still prohibitive, especially when tracking points densely in a video. We thus propose a new design, in which we introduce K *virtual tracks tokens*, where $K \ll N$ is a hyperparameter. These are just added as additional tokens to the input grid with a fixed, learnable initialization and removed at the output. They participate in time attention as regular tracks, and in cross attention with all other tracks, reducing the cost to $O(NK + K^2 + T^2)$.

Starting with DETR [6], various computer vision transformers have used learnable queries. For instance, [20] uses them to decode dense outputs. Our virtual tracks are different, however: they mirror and shadow the computation of the prediction targets (*i.e.*, the tracks), actively participating in the calculations to reduce the computational burden.

3.3. Windowed inference

A key advantage of formulating tracking as iterated updates is that it can easily support a sliding window application to process long videos. Consider in particular a video V of length $T' > T$ longer than the maximum window length T supported by the architecture. To track points throughout the entire video V , we split the video in $J = \lceil 2T'/T - 1 \rceil$ windows of length T , with an overlap of $T/2$ frames.¹

Let the superscript (m, j) denote the m -th application of the transformer to the j -th window. We thus have a $M \times J$ grid of quantities $(\hat{P}^{(m,j)}, \hat{v}^{(m,j)}, Q^{(m,j)})$, spanning transformer iterations and windows. Quantities $m = 0$ and $j = 1$ are initialized as for the single window case. Then, the transformer is applied M times to obtain the estimate $(M, 1)$. The latter is used to initialize estimate $(0, 2)$ by broadcasting the known quantities as before. Specifically, the first $T/2$ components of $\hat{P}^{(0,2)}$ are copies of the last $T/2$ components of $\hat{P}^{(M,1)}$; the last $T/2$ components of $\hat{P}^{(0,2)}$ are instead copies of the last time $t = T/2 - 1$ from $\hat{P}^{(M,1)}$. The same update rule is used for $\hat{v}^{(0,2)}$, while $Q^{(0,j)}$ is always initialized with initial track features Q . This process is repeated until estimate (M, J) is obtained.

¹We assume that T is even. The last window is shorter if $T/2$ does not divide T' .

3.4. Unrolled window training

We found it important to learn the windowed transformer in an unrolled fashion in order to learn to handle semi-overlapping windows. The primary loss is for track regression, summed over iterated transformer applications and windows:

$$\mathcal{L}_1(\hat{P}, P) = \sum_{j=1}^J \sum_{m=1}^M \gamma^{M-m} \|\hat{P}^{(m,j)} - P^{(j)}\|, \quad (2)$$

where $\gamma = 0.8$ discounts early transformer updates. Here $P^{(j)}$ contains the ground-truth trajectories restricted to window j (trajectories which start in the middle of the window are padded backwards). The second loss is the cross entropy of the visibility flags $\mathcal{L}_2(\hat{v}, v) = \sum_{j=1}^J \text{CE}(\hat{v}^{(M,j)}, v^{(j)})$. While only a moderate number of windows are used in the loss during training due to the computational cost, at test time we can unroll the windowed transformer applications arbitrarily, thus in principle handling any video length.

Implementation details. A technical difficulty is that the number of tracks N is not fixed, but varies from window to window as new points can be added to the tracker at any time. While conceptually this is handled by simply adding more tokens when needed, in practice changing the number of tokens makes batching data for training difficult. Instead, we allocate enough tokens to support all points that must be tracked, regardless of which window they are added in, and use masking to ignore tokens that are not yet used.

3.5. Support points

CoTracker can take advantage of tracking several points jointly. It is typical for applications to have several points to track, but in some cases, one might be interested in tracking a few or even a single point. In fact, single-point tracking is a case we consider in the evaluation for fairness (Sec. 1).

In practice, we found it beneficial to track additional ‘support points’ which are not explicitly requested by the user, particularly when the goal is to track only a few of them. Moreover, we have found that different configurations of such support points can lead to small differences

in performance. We experiment with various configuration types, visualized in Fig. 4. With the “global” strategy, the support points form a regular grid across the whole image. With the “local” strategy, the grid of points is centred around the point we wish to track, thus allowing the model to focus on a neighbourhood of it. We also test using the SIFT detector [26] to select support points. Note that these patterns are only considered at inference time and are used to improve the accuracy of the tracker for the target points.

4. Experiments

We thoroughly evaluate CoTracker on standard real and synthetic tracking benchmarks to assess its performance and generalization properties in difficult conditions and against numerous state-of-the-art trackers.

Single target tracks. We pay particular attention to the design of the evaluation protocol to ensure its fairness. Specifically, we note that existing benchmarks contain ground truth tracks which are concentrated on a few foreground objects, potentially revealing the presence of such objects to a joint tracker like ours. In order to ensure that no ground-truth information is leaked to our tracker, in the “single target track” protocol we track one benchmark point at a time, but automatically add additional support points (Sec. 3.5) to allow the model to perform joint tracking. In this way, our comparison is fair to single-point trackers. Furthermore, by comparing different configurations of such support tracks, we can better quantify the importance of joint tracking.

Datasets and evaluation protocol. We use **TAP-Vid** [10], a collection of four tracking benchmarks, three real ones for evaluation and a synthetic one for training. The latter is **TAP-Vid-Kubric**, also used by several prior works to train their trackers. It consists of sequences of 24 frames showing 3D rigid objects falling to the ground under gravity and bouncing, generated using the Kubric engine [14]. Point tracks are selected randomly, primarily on objects, and some on the background. Objects occlude each other and the background as they move.

For evaluation, we consider the *TAP-Vid-DAVIS* set, containing 30 real sequences of about 100 frames. Points are queried on random objects at random times and evaluation assesses both predictions of positions and visibility flags. This uses two evaluation protocols. In the “queried first” protocol, each point is queried only once in the video, at the first frame where it becomes visible. The tracker is expected to operate causally, predicting positions only for future frames. In the “queried strided” protocol, points are queried every five frames and tracking is bidirectional. Given that most trackers (ours, PIPs, PIPs++) are causal, we run them twice, on the video and its reverse. We assess tracking accuracy using the TAP-Vid metrics [10]: Occlusion Accuracy (OA; accuracy of occlusion prediction treated as binary

classification), $\delta_{\text{avg}}^{\text{vis}}$ (fraction of visible points tracked within 1, 2, 4, 8 and 16 pixels, averaged over thresholds), and Average Jaccard (AJ, measuring jointly geometric and occlusion prediction accuracy). Following [10], the $\delta_{\text{avg}}^{\text{vis}}$ and AJ tracking thresholds are applied after virtually resizing images to 256×256 pixels.

PointOdyssey [52] is a more recent synthetic benchmark dataset for long-term tracking. It contains 100 sequences several thousand frames long with objects and characters moving around the scene. Scenes are much more realistic than TAP-Vid-Kubric. We train and evaluate CoTracker on PointOdyssey and report $\delta_{\text{avg}}^{\text{vis}}$ and $\delta_{\text{avg}}^{\text{occ}}$, δ_{avg} . The last two are the same as $\delta_{\text{avg}}^{\text{vis}}$, but for occluded and all points, respectively; they can be computed because the dataset is synthetic so the ground-truth positions of invisible points are known. We also report their *Survival* rate, which is the average fraction of video frames until the tracker fails (detected when the tracking error exceeds 50 pixels).

Dynamic Replica [23] is a synthetic dataset for 3D reconstruction that contains long-term tracking annotations. It consists of 500 300-frame sequences of articulated models of people and animals. We measure $\delta_{\text{avg}}^{\text{vis}}$ and $\delta_{\text{avg}}^{\text{occ}}$ on the “valid” split of this dataset.

Implementation details. Here we provide important implementation details and refer to the sup. mat. for others. For **training**, we use 11,000 TAP-Vid-Kubric sequences of $T' = 24$ frames using sliding window size $T = 8$ and train for 50,000 iterations using 32 NVIDIA A100 80GB GPUs with the batch size of 1. Training tracks are sampled preferentially on objects. During training, we construct batches of 768 tracks out of 2048 among those that are visible either in the first or middle frames of the sequence to train the tracker to handle both cases. In a similar manner, we also train a second version of CoTracker on the train split of PointOdyssey, using 128 tracks randomly sampled from sequences of length $T' = 56$.

We **evaluate** joint tracking using different configurations of target and support points (Sec. 3.5 and Fig. 4). The natural choice is to jointly track *all* target points specified in a given benchmark sequence, which we test for all datasets. We also assess the benefits of adding various configurations of support points (Sec. 3.5). Furthermore, benchmark points might be biased for objects, which is particularly evident in TAP-Vid-DAVIS (Fig. 4). In order to assess CoTracker more fairly against single-point trackers, we thus also experiment with tracking a *single* target point at a time, plus various configurations of support points.

The video **resolution** can affect tracking performance substantially. For TAP-Vid-DAVIS, we follow their protocol and downsample videos to 256×256 , which ensures that no more information than expected is passed to the tracker. However, each tracker has a different native resolution at which it is trained on (384×512 for PIPs and CoTracker;

Method	Training data	DAVIS First			DAVIS Strided			Dynamic Replica		
		AJ \uparrow	$\delta_{\text{avg}}^{\text{vis}} \uparrow$	OA \uparrow	AJ \uparrow	$\delta_{\text{avg}}^{\text{vis}} \uparrow$	OA \uparrow	$\delta_{\text{avg}} \uparrow$	$\delta_{\text{avg}}^{\text{vis}} \uparrow$	$\delta_{\text{occ}}^{\text{avg}} \uparrow$
TAP-Net [10]	TAP-Vid-Kubric	33.0	48.6	78.8	38.4	53.1	82.3	45.5	53.3	20.0
OmniMotion [46]	—	—	—	—	51.7	67.5	85.3	—	—	—
PIPs [15]	FlyingThings++	42.2	64.8	77.7	52.4	70.0	83.6	41.0	47.1	21.0
MFT [31]	Kubric + others	47.3	66.8	77.8	56.1	70.8	86.9	—	—	—
PIPs++ [52]	PointOdyssey	—	69.1	—	—	73.7	—	55.5	64.0	28.5
TAPIR [11]	TAP-Vid-Kubric	56.2	70.0	86.5	61.3	73.6	88.8	56.8	66.1	27.2
CoTracker (Ours)	TAP-Vid-Kubric	62.2	75.7	89.3	65.9	79.4	89.9	61.6	68.9	37.6

Table 1. **State of the art comparison.** We compare CoTracker to the best trackers available on TAP-Vid-DAVIS utilizing both their “queried first” and “queried strided” evaluation protocols as well as on Dynamic Replica. During evaluation on DAVIS, TAPIR and PIPs++ have access to all the video frames at once, while we process videos in an online manner, using a causal sliding window.



Figure 5. **Qualitative Results.** For PIPs++ (top), many points are incorrectly tracked and end up being ‘stuck’ on the front of the car. TAPIR (middle) works well for visible points but fails to handle occluded points. As soon as a point becomes occluded, it starts moving chaotically around the image. Our CoTracker (bottom) produces cleaner tracks. The tracks are also more ‘linear’ than those of PIPs++ or TAPIR, which is accurate as the primary motion is a homography (the observer does not translate).

Method	PointOdyssey			
	$\delta_{\text{avg}} \uparrow$	$\delta_{\text{avg}}^{\text{vis}} \uparrow$	$\delta_{\text{avg}}^{\text{occ}} \uparrow$	Survival \uparrow
TAP-Net [10]	28.4	—	—	18.3
PIPs [16]	27.3	—	—	42.3
PIPs++ [†] [52]	29.0	32.4	18.8	47.0
CoTracker (Ours)	30.2	32.7	24.2	55.2

Table 2. **PointOdyssey.** All methods are trained on PointOdyssey. [†] results for [52] obtained using released code and model.

512 \times 896 for PIPs++); We thus resize videos to the native resolution of each tracker before running it. For Dynamic

Replica and PointOdyssey, we resize videos to the native tracker resolution, as there is no prescribed resolution.

4.1. Results

Is joint tracking beneficial? In Tab. 3 we demonstrate the importance of tracking points jointly, which is the main motivation of CoTracker. This is achieved by removing cross-track attention from the tracker, thus ignoring the correlation between tracks entirely. For fairness, we maintain the same model size and replace the six cross-track attention layers with twelve time attention layers. We test on TAP-Vid-DAVIS tracking either a *single* target point at a time or *all* target points simultaneously. We also test different configurations of support points (Sec. 3.5 and Fig. 4): none,

	Attention		Points		DAVIS First		
	time	joint	target	support	AJ \uparrow	δ_{avg} \uparrow	OA \uparrow
(a)	✓	✗	single	—	58.3	71.5	86.4
(b)	✓	✓	single	—	41.1	62.9	75.1
(c)	✓	✓	single	glob. 9×9	56.8	71.2	85.8
(d)	✓	✓	single	SIFT 8×8	57.4	72.1	85.8
(e)	✓	✓	single	loc. 10×10	60.4	75.2	87.5
(f)	✓	✓	single	glob. 5×5 +loc. 8×8	62.2	75.7	89.3
(g)	✓	✓	all	—	57.6	73.2	86.1
(h)	✓	✓	all	glob. 5×5	60.5	75.8	87.6
(i)	✓	✓	all	SIFT 8×8	60.7	75.7	88.1

Table 3. **Importance of joint tracking.** We compare using time and cross-track attention, tracking single or multiple target points, and using additional support points.

Unrolled Training	DAVIS First		
	AJ \uparrow	δ_{avg} \uparrow	OA \uparrow
✗	44.6	60.5	75.3
✓	62.2	75.7	89.3

Table 4. **Unrolled training.** CoTracker is built for sliding window predictions. Using them during training is important.

Num. virt. tracks	DAVIS First			Max. num. tracks	Time [s]
	AJ \uparrow	δ_{avg} \uparrow	OA \uparrow		
0	61.6	75.6	88.3	97×97	207.3
32	60.2	74.4	88.5	263×263	26.8
64	62.2	75.7	89.3	263×263	27.9
128	60.9	74.8	88.4	263×263	30.1

Table 5. The **virtual tracks** allow CoTracker to scale. We report the maximum number of tracks that can fit on a 80 GB GPU.

global, global and local, global and SIFT grids. We test grids of different sizes, ranging from 1×1 to 10×10 , and for the sake of compactness, we report the best settings.

We find that: (1) for the same number of parameters, tracking points jointly instead of independently is significantly better (+3.9 AJ (a) to (f)); (2) when tracking single target points, adding support points in a global grid significantly boosts performance (+15 AJ (b) to (c)); (3) the latter is further improved by using a global/local grid (+5.4 AJ (c) to (f)); (4) the SIFT grid is less good than the global/local grid (-4.8 AJ (f) to (c)), but slightly better than the global alone (+0.6 AJ (c) to (d)); (5) adding support points to all target points is better (+2.9 AJ (g) to (i)). This demonstrates that *tracking points jointly is highly beneficial* in all cases.

How does CoTracker compare to prior work? Using configuration (f) from Tab. 3, in Tab. 1 we compare CoTracker to state-of-the-art trackers on three benchmark datasets, improving all metrics by substantial margins in all cases. Note that, for TAP-Vid-DAVIS, we assess tracking a single target point at a time, plus support points, which is fair to single-point trackers. Hence, *the method advances the state of the art.*

Is unrolled training important? We design CoTracker for tracking in a windowed manner, and in Tab. 4 we thus assess the effect of unrolling windows during training (Sec. 3.4). Switching off unrolled training decreases performance by 18 AJ points, meaning that unrolled training helps to track over long periods of time, $> 10 \times$ longer than the sequences used in training. Hence, *unrolled training is important.*

Do virtual tracks help CoTracker to scale? In Sec. 4, we assess the benefits of using virtual tracks. For a fixed memory budget (80 GB), using virtual tracks allows us to track $\times 7.4$ more point points than without them; in fact, we can track a whole 263×263 grid, which is quasi-dense for the input video resolution. The number of virtual tracks does not affect scalability, but affects performance, with the best results obtained using 64 virtual tracks. The overall accuracy is also *better* when many tracks are utilized as it plays on the strengths of the joint tracker. Hence, *virtual tracks allow to track almost one order of magnitude more tracks.*

4.2. Limitations

While better than other tracker, CoTracker still makes tracking mistakes that would be easily avoided by a human. Another limitation is that it still processes relatively short windows of points at a time, and thus can fail for points that stay occluded for the length of multiple sliding windows. For the same reason, it can fail to track points for thousands of frames. While joint tracking and unrolled training mitigate this, offline applications of the tracker would benefit from considering all video frames at once.

5. Conclusions

We have presented CoTracker, a transformer-based point tracker that tracks several points jointly, accounting for their correlation. CoTracker is state-of-the-art on the standard tracking benchmarks, often by a substantial margin, can track through occlusions and when points leave the field of view, even for hundreds of frames, can track very diverse configurations of points (target and support), and can track a very large number of points simultaneously. The transformer architecture is flexible and future extensions could integrate more functionalities, such as 3D reconstruction.

6. Acknowledgments

We would like to thank Luke Melas-Kyriazi for his paper comments, Jianyuan Wang, Roman Shapovalov, Luke Melas-Kyriazi and Adam W. Harley for the insightful discussions. Christian Rupprecht is supported by ERC-CoG UNION101001212 and VisualAI EP/T028572/1.

References

- [1] Gedas Bertasius, Heng Wang, and Lorenzo Torresani. Is space-time attention all you need for video understanding? In *Proc. ICML*, July 2021. [4](#)
- [2] Stanley T Birchfield and Shrinivas J Pundlik. Joint tracking of features and edges. In *Proc. CVPR*, 2008. [2](#)
- [3] M. J. Black and P. Anandan. A framework for the robust estimation of optical flow. In *Proc. ICCV*, 1993. [2](#)
- [4] Andrés Bruhn, Joachim Weickert, and Christoph Schnörr. Lucas/kanade meets horn/schunck: Combining local and global optic flow methods. *IJCV*, 61, 2005. [2](#)
- [5] Daniel J Butler, Jonas Wulff, Garrett B Stanley, and Michael J Black. A naturalistic open source movie for optical flow evaluation. In *Proc. ECCV*, 2012. [3](#)
- [6] Nicolas Carion, Francisco Massa, Gabriel Synnaeve, Nicolas Usunier, Alexander Kirillov, and Sergey Zagoruyko. End-to-end object detection with transformers. In *Proc. ECCV*, 2020. [5](#)
- [7] Joao Carreira and Andrew Zisserman. Quo vadis, action recognition? a new model and the kinetics dataset. In *Proc. CVPR*, 2017. [12](#)
- [8] Fei Chen, Xiaodong Wang, Yunxiang Zhao, Shaohe Lv, and Xin Niu. Visual object tracking: A survey. *CVIU*, 222, 2022. [2](#)
- [9] Toshio M Chin, William Clement Karl, and Alan S Willsky. Probabilistic and sequential computation of optical flow using temporal coherence. *IEEE Trans. on Image Processing*, 3(6), 1994. [2](#)
- [10] Carl Doersch, Ankush Gupta, Larisa Markeeva, Adrià Recasens, Lucas Smaira, Yusuf Aytar, João Carreira, Andrew Zisserman, and Yi Yang. Tap-vid: A benchmark for tracking any point in a video. *arXiv*, 2022. [2](#), [3](#), [6](#), [7](#), [11](#), [12](#)
- [11] Carl Doersch, Yi Yang, Mel Vecerik, Dilara Gokay, Ankush Gupta, Yusuf Aytar, Joao Carreira, and Andrew Zisserman. Tapir: Tracking any point with per-frame initialization and temporal refinement, 2023. [1](#), [3](#), [7](#), [12](#)
- [12] Alexey Dosovitskiy, Philipp Fischer, Eddy Ilg, Philip Hausser, Caner Hazirbas, Vladimir Golkov, Patrick Van Der Smagt, Daniel Cremers, and Thomas Brox. FlowNet: Learning optical flow with convolutional networks. In *Proc. ICCV*, 2015. [2](#), [3](#)
- [13] Michael Elad and Arie Feuer. Recursive optical flow estimation—adaptive filtering approach. *J. of Visual Communication and Image Representation*, 9(2), 1998. [2](#)
- [14] Klaus Greff, Francois Belletti, Lucas Beyer, Carl Doersch, Yilun Du, Daniel Duckworth, David J Fleet, Dan Gnanaprasam, Florian Golemo, Charles Herrmann, Thomas Kipf, Abhijit Kundu, Dmitry Lagun, Issam Laradji, Hsueh-Ti (Derek) Liu, Henning Meyer, Yishu Miao, Derek Nowrouzezahrai, Cengiz Oztireli, Etienne Pot, Noha Radwan, Daniel Rebaï, Sara Sabour, Mehdi S. M. Sajjadi, Matan Sela, Vincent Sitzmann, Austin Stone, Deqing Sun, Suhani Vora, Ziyu Wang, Tianhao Wu, Kwang Moo Yi, Fangcheng Zhong, and Andrea Tagliasacchi. Kubric: a scalable dataset generator. In *Proc. CVPR*, 2022. [6](#)
- [15] Adam W Harley, Zhaoyuan Fang, and Katerina Fragkiadaki. Particle video revisited: Tracking through occlusions using point trajectories. In *Proc. ECCV*, 2022. [2](#), [3](#), [7](#), [12](#)
- [16] Adam W. Harley, Zhaoyuan Fang, and Katerina Fragkiadaki. Particle videos revisited: Tracking through occlusions using point trajectories. *arXiv.cs, abs/2204.04153*, 2022. [7](#)
- [17] Berthold KP Horn and Brian G Schunck. Determining optical flow. *Artificial intelligence*, 17(1-3), 1981. [2](#)
- [18] Zhaoyang Huang, Xiaoyu Shi, Chao Zhang, Qiang Wang, Ka Chun Cheung, Hongwei Qin, Jifeng Dai, and Hongsheng Li. Flowformer: A transformer architecture for optical flow. In *Proc. ECCV*, 2022. [2](#)
- [19] Eddy Ilg, Nikolaus Mayer, Tonmoy Saikia, Margret Keuper, Alexey Dosovitskiy, and Thomas Brox. FlowNet 2.0: Evolution of optical flow estimation with deep networks. In *Proc. CVPR*, 2017. [2](#)
- [20] Andrew Jaegle, Sebastian Borgeaud, Jean-Baptiste Alayrac, Carl Doersch, Catalin Ionescu, David Ding, Skanda Koppula, Daniel Zoran, Andrew Brock, Evan Shelhamer, Olivier J. Hénaff, Matthew M. Botvinick, Andrew Zisserman, Oriol Vinyals, and João Carreira. Perceiver IO: A general architecture for structured inputs & outputs. In *Proc. ICLR*, 2022. [2](#), [5](#)
- [21] Joel Janai, Fatma Guney, Anurag Ranjan, Michael Black, and Andreas Geiger. Unsupervised learning of multi-frame optical flow with occlusions. In *Proc. ECCV*, 2018. [2](#)
- [22] Shihao Jiang, Yao Lu, Hongdong Li, and Richard Hartley. Learning optical flow from a few matches. In *Proc. CVPR*, 2021. [2](#)
- [23] Nikita Karaev, Ignacio Rocco, Benjamin Graham, Natalia Neverova, Andrea Vedaldi, and Christian Rupprecht. DynamicStereo: Consistent dynamic depth from stereo videos. In *Proceedings of the IEEE Conference on Computer Vision and Pattern Recognition (CVPR)*, 2023. [2](#), [6](#)
- [24] Nikita Karaev, Ignacio Rocco, Benjamin Graham, Natalia Neverova, Andrea Vedaldi, and Christian Rupprecht. Dynamicstereo: Consistent dynamic depth from stereo videos. In *Proc. CVPR*, 2023. [3](#)
- [25] Ilya Loshchilov and Frank Hutter. Decoupled weight decay regularization. *arXiv preprint arXiv:1711.05101*, 2017. [13](#)
- [26] David G. Lowe. Distinctive image features from scale-invariant keypoints. *IJCV*, 60(2), 2004. [6](#), [11](#)
- [27] Bruce D Lucas and Takeo Kanade. An iterative image registration technique with an application to stereo vision. In *Proc. IJCAI*, volume 2, 1981. [2](#)
- [28] Jianqin Luo, Zhexiong Wan, Bo Li, Yuchao Dai, et al. Continuous parametric optical flow. In *Thirty-seventh Conference on Neural Information Processing Systems*, 2023. [2](#)
- [29] Lain Matthews, Takahiro Ishikawa, and Simon Baker. The template update problem. *PAMI*, 26(6), 2004. [2](#)
- [30] Nikolaus Mayer, Eddy Ilg, Philip Hausser, Philipp Fischer, Daniel Cremers, Alexey Dosovitskiy, and Thomas Brox. A large dataset to train convolutional networks for disparity, optical flow, and scene flow estimation. In *Proc. CVPR*,

2016. [3](#)
- [31] Michal Neoral, Jonáš Šerých, and Jiří Matas. Mft: Long-term tracking of every pixel, 2023. [2](#), [7](#)
- [32] Jordi Pont-Tuset, Federico Perazzi, Sergi Caelles, Pablo Arbeláez, Alex Sorkine-Hornung, and Luc Van Gool. The 2017 davis challenge on video object segmentation. *arXiv*, 2017. [1](#)
- [33] Zhile Ren, Orazio Gallo, Deqing Sun, Ming-Hsuan Yang, Erik B Sudderth, and Jan Kautz. A fusion approach for multi-frame optical flow estimation. In *Proc. WACV*, 2019. [2](#)
- [34] Peter Sand and Seth Teller. Particle video: Long-range motion estimation using point trajectories. *IJCV*, 80, 2008. [2](#)
- [35] Xiaoyu Shi, Zhaoyang Huang, Weikang Bian, Dasong Li, Manyuan Zhang, Ka Chun Cheung, Simon See, Hongwei Qin, Jifeng Dai, and Hongsheng Li. Videoflow: Exploiting temporal cues for multi-frame optical flow estimation. *arXiv*, 2023. [2](#)
- [36] Xiaoyu Shi, Zhaoyang Huang, Dasong Li, Manyuan Zhang, Ka Chun Cheung, Simon See, Hongwei Qin, Jifeng Dai, and Hongsheng Li. Flowformer++: Masked cost volume autoencoding for pretraining optical flow estimation. *arXiv*, 2023. [2](#)
- [37] Hedvig Sidenbladh, Michael J Black, and David J Fleet. Stochastic tracking of 3d human figures using 2d image motion. In *Proc. ECCV*, 2000. [2](#)
- [38] Leslie N Smith and Nicholay Topin. Super-convergence: Very fast training of neural networks using large learning rates. In *Artificial intelligence and machine learning for multi-domain operations applications*, volume 11006, pages 369–386. SPIE, 2019. [13](#)
- [39] Xiuchao Sui, Shaohua Li, Xue Geng, Yan Wu, Xinxing Xu, Yong Liu, Rick Goh, and Hongyuan Zhu. Craft: Cross-attentional flow transformer for robust optical flow. In *Proc. CVPR*, 2022. [2](#)
- [40] Deqing Sun, Daniel Vlastic, Charles Herrmann, Varun Jampani, Michael Krainin, Huiwen Chang, Ramin Zabih, William T Freeman, and Ce Liu. Autoflow: Learning a better training set for optical flow. In *Proc. CVPR*, 2021. [3](#)
- [41] Deqing Sun, Xiaodong Yang, Ming-Yu Liu, and Jan Kautz. Pwc-net: Cnns for optical flow using pyramid, warping, and cost volume. In *Proc. CVPR*, 2018. [2](#)
- [42] Shangkun Sun, Yuanqi Chen, Yu Zhu, Guodong Guo, and Ge Li. Skflow: Learning optical flow with super kernels. *arXiv*, 2022. [2](#)
- [43] Zachary Teed and Jia Deng. Raft: Recurrent all-pairs field transforms for optical flow. In *Proc. ECCV*, 2020. [2](#), [4](#)
- [44] Ashish Vaswani, Noam Shazeer, Niki Parmar, Jakob Uszkoreit, Llion Jones, Aidan N Gomez, Łukasz Kaiser, and Illia Polosukhin. Attention is all you need. In *Proc. NeurIPS*, 2017. [2](#)
- [45] Jianyuan Wang, Yiran Zhong, Yuchao Dai, Kaihao Zhang, Pan Ji, and Hongdong Li. Displacement-invariant matching cost learning for accurate optical flow estimation. *Proc. NeurIPS*, 33, 2020. [2](#)
- [46] Qianqian Wang, Yen-Yu Chang, Ruojin Cai, Zhengqi Li, Bharath Hariharan, Aleksander Holynski, and Noah Snavely. Tracking everything everywhere all at once, 2023. [3](#), [7](#)
- [47] Haofei Xu, Jiaolong Yang, Jianfei Cai, Juyong Zhang, and Xin Tong. High-resolution optical flow from 1d attention and correlation. In *Proc. CVPR*, 2021. [2](#)
- [48] Jia Xu, Rene Ranftl, and Vladlen Koltun. Accurate optical flow via direct cost volume processing. In *Proc. CVPR*, July 2017. [2](#)
- [49] Feihu Zhang, Oliver J Woodford, Victor Adrian Prisacariu, and Philip HS Torr. Separable flow: Learning motion cost volumes for optical flow estimation. In *Proc. CVPR*, 2021. [2](#)
- [50] Shiyu Zhao, Long Zhao, Zhixing Zhang, Enyu Zhou, and Dimitris Metaxas. Global matching with overlapping attention for optical flow estimation. In *Proc. CVPR*, 2022. [2](#)
- [51] Tao Zhao and Ramakant Nevatia. Tracking multiple humans in crowded environment. In *Proc. CVPR*, volume 2, 2004. [2](#)
- [52] Yang Zheng, Adam W Harley, Bokui Shen, Gordon Wetstein, and Leonidas J Guibas. Pointodyssey: A large-scale synthetic dataset for long-term point tracking. In *Proceedings of the IEEE/CVF International Conference on Computer Vision*, pages 19855–19865, 2023. [1](#), [2](#), [3](#), [6](#), [7](#), [12](#)

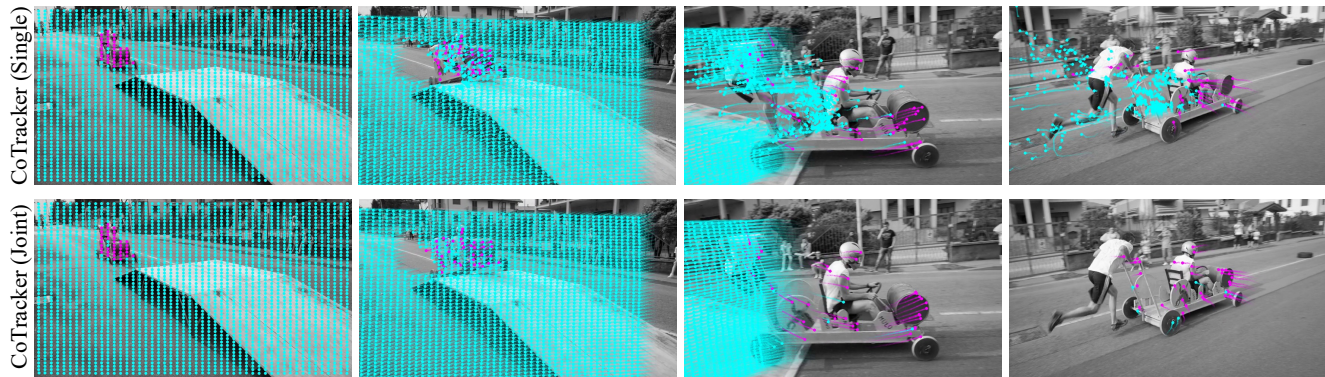


Figure 6. **Single point vs. joint tracking.** We qualitatively compare tracking individual points (top row) to tracking all points together (bottom). Background points are colored cyan while foreground points are magenta. We find that single-point tracking leads to background points following the object motion, as the model cannot reason well about the global context of the video (cyan points in later frames). Tracking points together results in better tracks for foreground and background points.

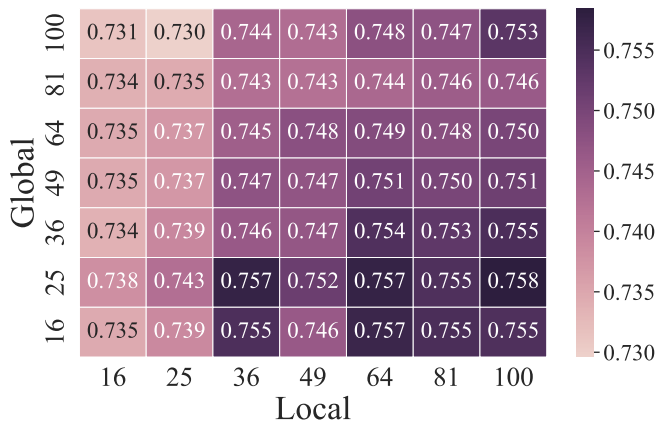


Figure 7. **Number of points.** Accuracy for additional global grid and local grid points. We compute δ_{avg}^{vis} on TAP-Vid-DAVIS to find the optimal grid sizes. We use 25 & 64 because of speed and higher occlusion accuracy (89.3 vs. 88.7).

A. Additional ablations

Here we provide additional ablation experiments that supplement the model choices from the main paper.

Single vs. joint point tracking. In Fig. 6, we demonstrate the importance of joint tracking. We track a grid of points starting at the first frame and compare CoTracker trained with and without cross-track attention. Joint tracking provides a global context and allows for better reasoning about the positions of occluded points.

Support points. We test different configurations of support points in Fig. 8. While adding SIFT [26] support points is better than sampling points uniformly on a global regular grid, adding a local grid yields significantly better results. The combination of global and local grids is slightly better, and in Fig. 7 we further test this combination with

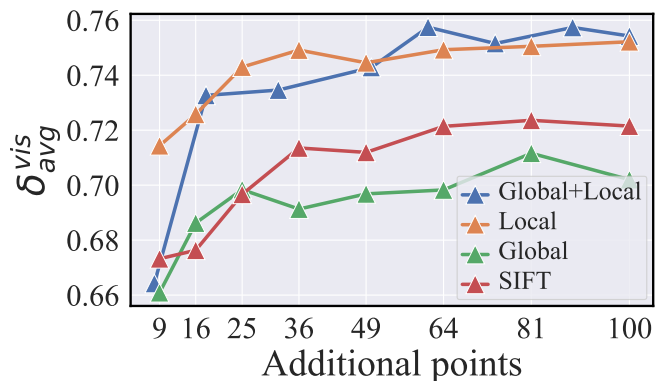


Figure 8. **Accuracy on TAP-Vid-DAVIS** depending on the number of additional local, global grid and SIFT points. When combining point sources, we use (close to) the same number of points.

different grid sizes ranging from 4×4 to 10×10 . We find that a configuration of 25 global and 64 local points is optimal for TAP-Vid-DAVIS in terms of speed and accuracy. While there are differences in performance across these hyper-parameters, the overall impact on performance is less than one percentage point for a wide variety of configurations.

Training sliding window size. In, Tab. 6 we ablate the sliding window size during training. While CoTracker can benefit from larger window sizes, the length of our training sequences from Kubric [10] is limited to 24 frames. Therefore, there is a trade-off between the context length and the ability to propagate predictions to future sliding windows. A sliding window of 8 is optimal for our training dataset.

Inference sliding window size. In Tab. 7, we examine the impact of the sliding window size on the performance of a model trained with a sliding window of $T = 8$. We find that

Window size	DAVIS First		
	AJ	$< \delta_{avg}^x$	OA
4	56.7	73.1	86.5
8	62.2	75.7	89.3
16	61.1	75.5	88.4

Table 6. **Training sliding window size.** We train and evaluate CoTracker with varying window lengths. As the training data only contains sequences of length 24, the model does not benefit from training with a bigger sliding window.

Window size	DAVIS First		
	AJ	$< \delta_{avg}^x$	OA
4	54.9	70.8	83.2
8	62.2	75.7	89.3
16	54.6	68.8	82.9

Table 7. **Inference sliding window size.** The model is trained with sliding window size $T = 8$. The same window size gives the best results.

the model performs best when the training and evaluation window sizes are identical.

B. Efficiency

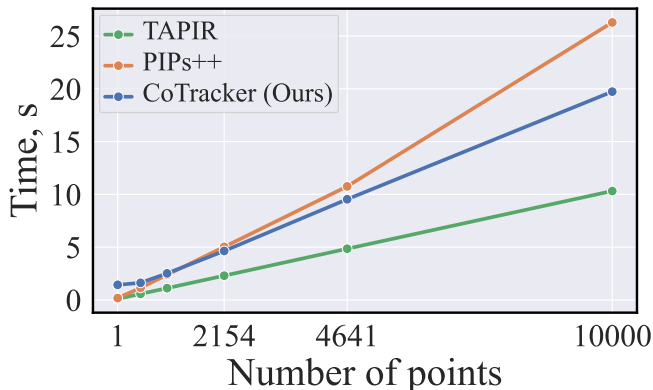


Figure 9. **Efficiency.** We track N points sampled on the first frame of a 50-frame video of resolution 256×256 using a NVIDIA A40 48GB GPU, and report the time it takes the method to process the video.

In Fig. 9 we evaluate efficiency of PIPs++ [52], TAPIR [11] and CoTracker on a 50-frame video of resolution 256×256 by running them on a A40 GPU. We track points sampled on a regular grid at the first frame of the video and report the time it takes to process the entire video sequence. CoTracker is slower than TAPIR but faster than PIPs++ (while achieving better accuracy than both).

Stride	Kinetics First		
	AJ	δ_{avg}^{vis}	OA
PIPs++	—	58.5	—
TAPIR	49.6	64.2	85.0
CoTracker (Ours)	48.8	64.5	85.8

Table 8. **Evaluation on TAP-Vid Kinetics.**

Stride	DAVIS First		
	AJ	δ_{avg}^{vis}	OA
8	52.5	68.6	85.7
4	62.2	75.7	89.3

Table 9. **Feature stride ablation.** Higher resolution features help to make much more accurate predictions.

C. Evaluation on TAP-Vid-Kinetics

In Tab. 8 we evaluate CoTracker on TAP-Vid-Kinetics, a dataset of 1144 videos of approximately 250 frames each from Kinetics [7]. Some of these videos are discontinuous, i.e., they are composed of continuous video chunks. CoTracker is designed for continuous videos, and TAPIR contains a matching stage inspired by TAP-Net [10], which can help with such combined video chunks. This is why the performance gap between TAPIR and CoTracker for this benchmark is smaller than for other benchmarks.

D. Implementation Details

In this section, we complete the description of implementation details from the main paper. We will release the code and models with the paper.

Feature CNN. Given a sequence of T' frames with a resolution of 384×512 , we compute features for each frame using a 2-dimensional CNN. This CNN downsamples the input image by a factor of 4 (feature stride) and outputs features with 128 channels. Our CNN is the same as the one used in PIPs [15]. It consists of one 7×7 convolution with a stride of 2, eight residual blocks with 3×3 kernels and instance normalization, and two final convolutions with 3×3 and 1×1 kernels. In Tab. 9, we train CoTracker with two different feature downsampling factors (strides).

Sliding windows. When passing information from one sliding window to the next, we concatenate binary masks of shape (N, T) with visibility logits that indicate where the model needs to make predictions. For example, masks in the first sliding window would be equal to 1 from the frame where we start tracking the point, and 0 before that. Masks for all the subsequent sliding windows will be equal to 1 for the first overlapping $T/2$ frames, and 0 for the remaining

$T/2$. During training, tracking starts either from the first or from a random frame where the point is visible. If a point is not yet visible in the current sliding window, it will be masked out during the application of cross-track attention.

Iterative updates. We train the model with $M = 4$ iterative updates and evaluate it with $M = 6$. This setting provides a reasonable trade-off between speed and accuracy, as evaluated in Fig. 10. Interestingly, the performance remains stable for 4-8 iterative updates and begins to degrade slowly thereafter.

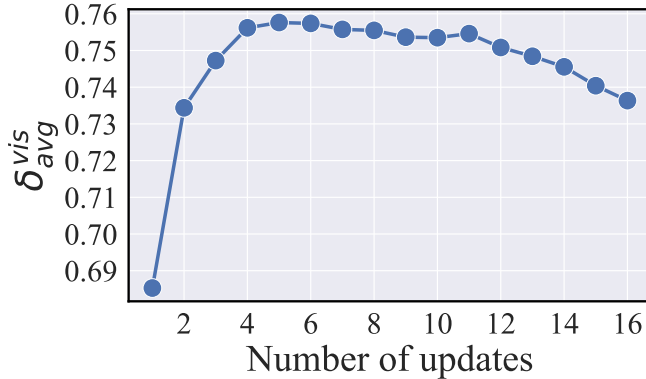


Figure 10. **Inference iterative updates.** We ablate the number of iterative updates M during inference. The network is trained with $M = 4$.

Training. CoTracker is trained with a batch size of 32, distributed across 32 GPUs. After applying data augmentations, we randomly sample 768 trajectories for each batch, with points visible either in the first or in the middle frame. We train the model for 50,000 iterations with a learning rate of $5e^{-4}$ and a linear 1-cycle [38] learning rate schedule, using the AdamW [25] optimizer.

Augmentations. During training, we employ Color Jitter and Gaussian Blur to introduce color and blur variations. We augment occlusions by either coloring a randomly chosen rectangular patch with its mean color or replacing it with another patch from the same image. Random scaling across height and width is applied to each frame to add diversity.

E. Broader societal impact

Motion estimation, whether in the guise of point tracking or optical flow, is a fundamental, low-level computer vision task. Many other tasks in computer vision build on it, from 3D reconstruction to video object segmentation. Ultimately, motion estimation algorithms are an important components of a very large number of applications of computer vision in many different areas. Point tracking has no *direct* societal impact; however, positive or negative effects on society can

materialise through its use in other algorithms, depending on the final application.